nature structural & molecular biology

SUPPLEMENTARY INFORMATION

https://doi.org/10.1038/s41594-019-0248-4

In the format provided by the authors and unedited.

Cryo-EM structures of four polymorphic TDP-43 amyloid cores

Qin Cao[1,3], David R. Boyer[1,3], Michael R. Sawaya[1], Peng Ge[2] and David S. Eisenberg[1]*

[1]Department of Chemistry and Biochemistry and Biological Chemistry, UCLA-DOE Institute, Molecular Biology Institute, and Howard Hughes Medical Institute, UCLA, Los Angeles, CA, USA. [2]California NanoSystem Institute, UCLA, Los Angeles, CA, USA. [3]These authors contributed equally: Qin Cao, David R. Boyer. *e-mail: david@mbi.ucla.edu

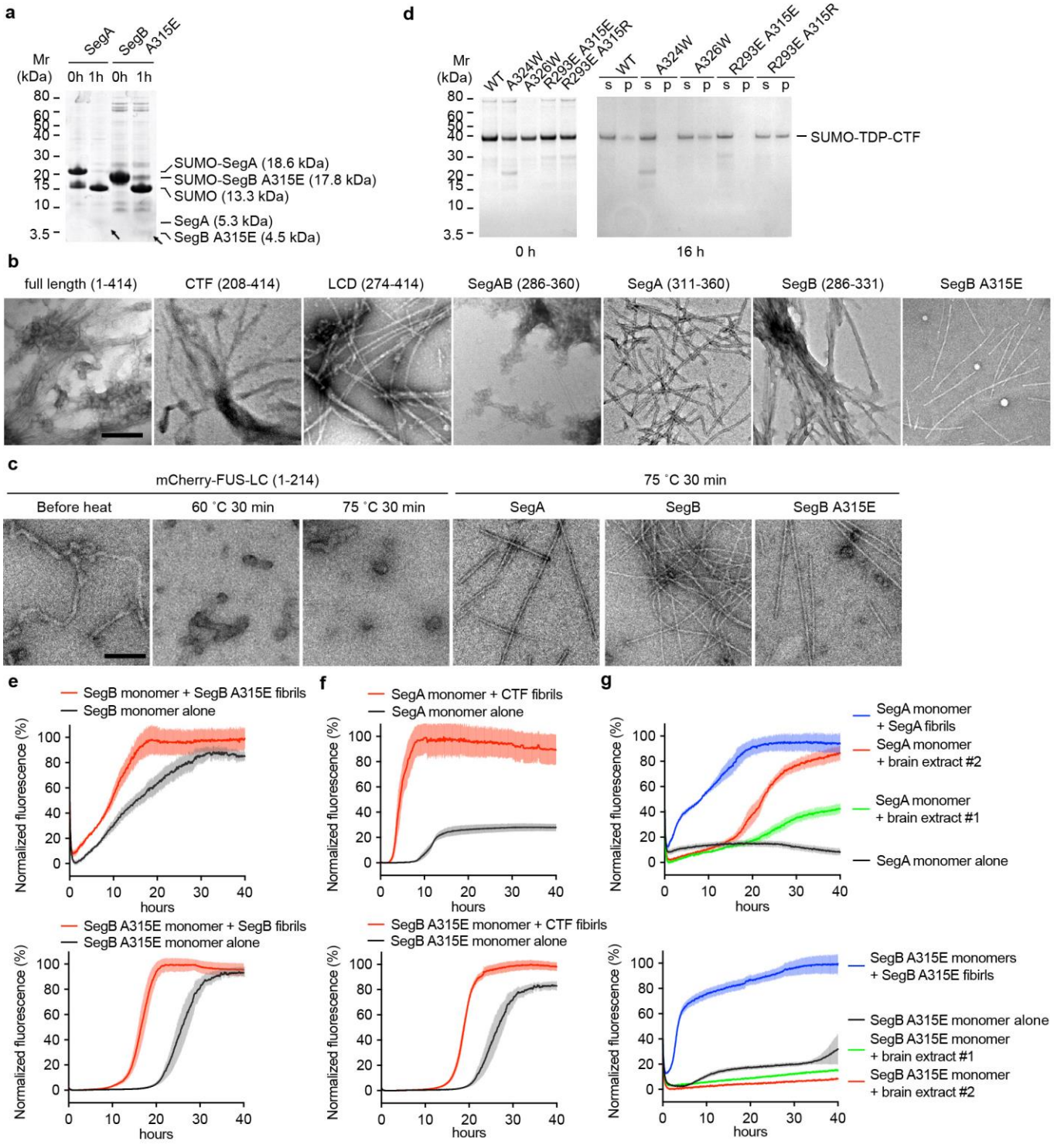

Supplementary Figure 1

Biochemical characterization of TDP-43 segments.

a, SDS-PAGE shows the cleavage of SegA and SegB A315E. SUMO-tagged segments are purified with Ni-column, and mixed with protease UPL1 to remove SUMO tag (0h). After 1 hour of cleavage (1h), bands corresponding to SUMO tag alone and TDP-43 segments (indicated by arrows) are shown on the gel, indicating successful cleavage. **b & c,** Negative stain electron microscope (EM) images of fibrils formed by TDP-43 segments (b) without heating or (c) heated before EM sample preparation. Fibrils of mCherry-FUS-LCD with or without heating were also observed with EM as a control. (Scale bar = 200 nm) Notice that the amount of fibrils in each image does not necessary corresponding to the total amount of fibrils in each sample, since the distribution of fibrils on EM grids was not even, especially for clumped fibrils. **d,** Aggregation assays of the pathological fragment TDP-CTF (208-414). Wild type (WT) and mutant TDP-CTFs conjugated with SUMO tags were incubated at 4 °C overnight. Samples were separated into supernatant (s) and pellet (p) by centrifugation and analyzed by SDS-PAGE. Notice that TDP-CTF A326W and R293E-A315R behave similarly as TDP-CTF WT, whereas the other two mutants show reduced aggregation. **e-g**, ThT aggregation curves of TDP-43 segments with or without seeding. Data are shown as mean ± s.d., n=4 independent experiments.

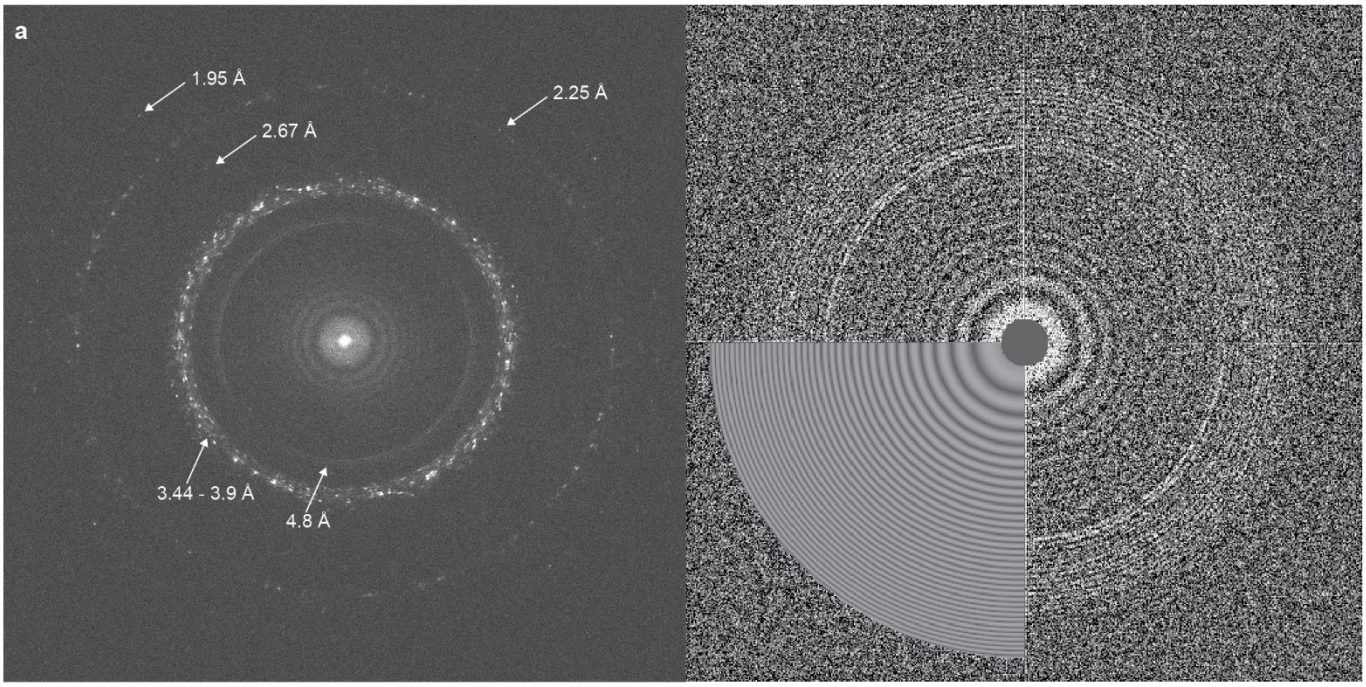

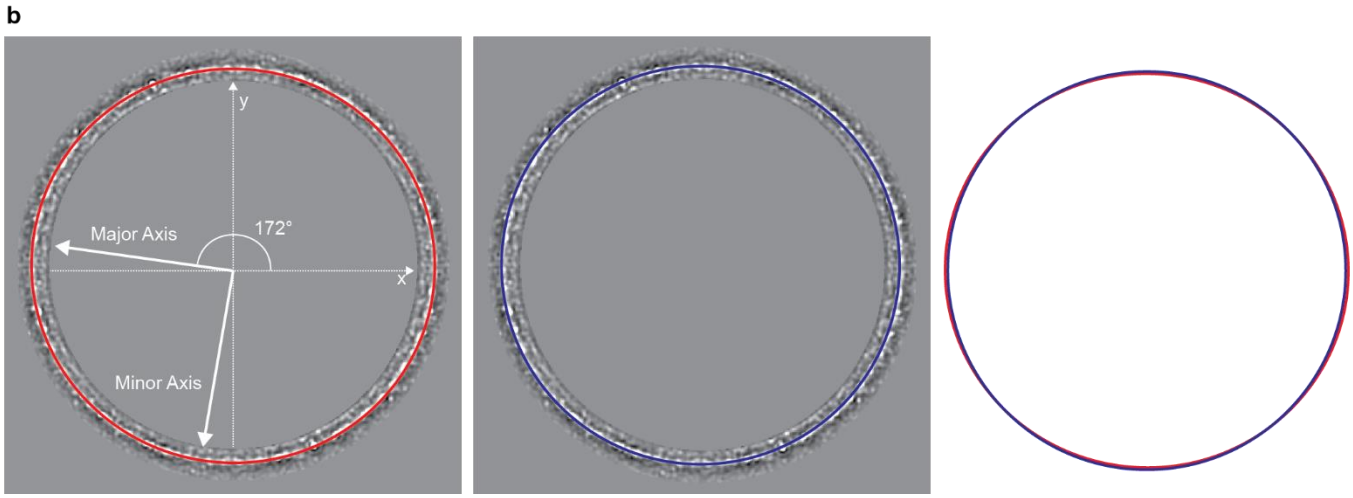

Supplementary Figure 2

Alignment of Titan Krios microscope.

a, (Left) Computed diffraction pattern from a micrograph containing crystalline ice with reflections visible to 1.95 Å demonstrating proper alignment of the microscope. (Right) Representative CTFFIND4 diagnostic image. **b,** Representative estimation and correction of anisotropic magnification distortion.

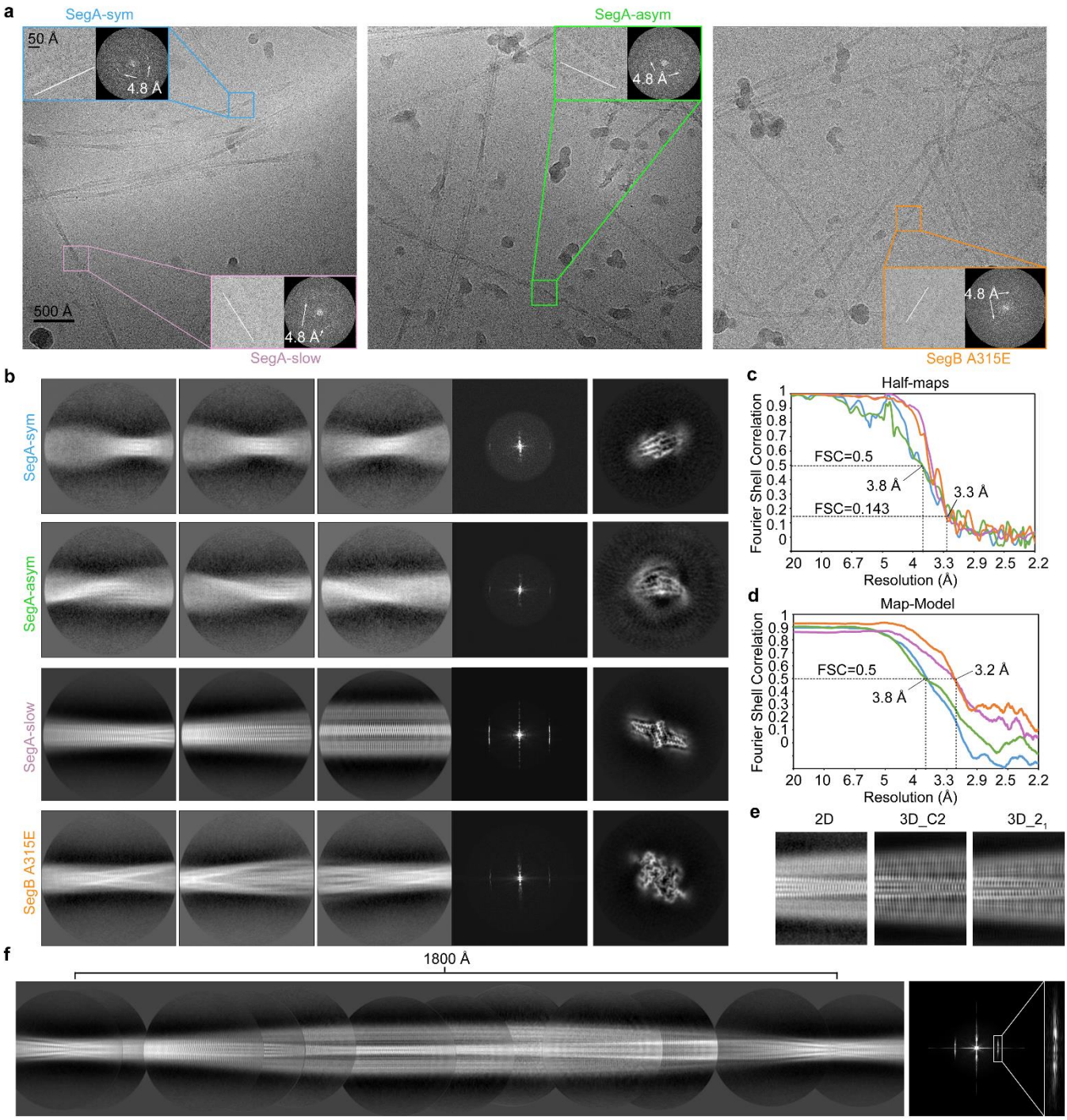

Supplementary Figure 3

Cryo-EM data processing.

a, Two (left and middle panel) and one (right) representative micrographs from data collection of SegA and SegB A315E, respectively. For each structure, a representative particle and its computed diffraction pattern are shown in the inset. The white line in each particle image indicates the direction of the fibril axis. The 4.8 Å reflection in the diffraction pattern corresponds to the helical rise. **b,** (left) Representative 2D class averages, (middle) computed diffraction pattern from 2D class, and (right) central slice from the final

reconstruction of each structure. **c**-**d,** FSC curves between two half-maps (**c**) and the cryo-EM reconstruction and refined atomic model (**d**) for each structure, using the same color coding as in (a) and (b). **e,** Comparison of 2D class average (left) and projection of 3D reconstruction from the same orientation of SegA-slow, when using C2 (middle) or pseudo-2_1 (right) symmetry for reconstruction. **f,** Manually assembled full pitch of SegA-slow from 2D class averages and its computed diffraction pattern with the 4.8 Å region enlarged confirms the presence of C_n rotational symmetry due to a reflection at n=0.

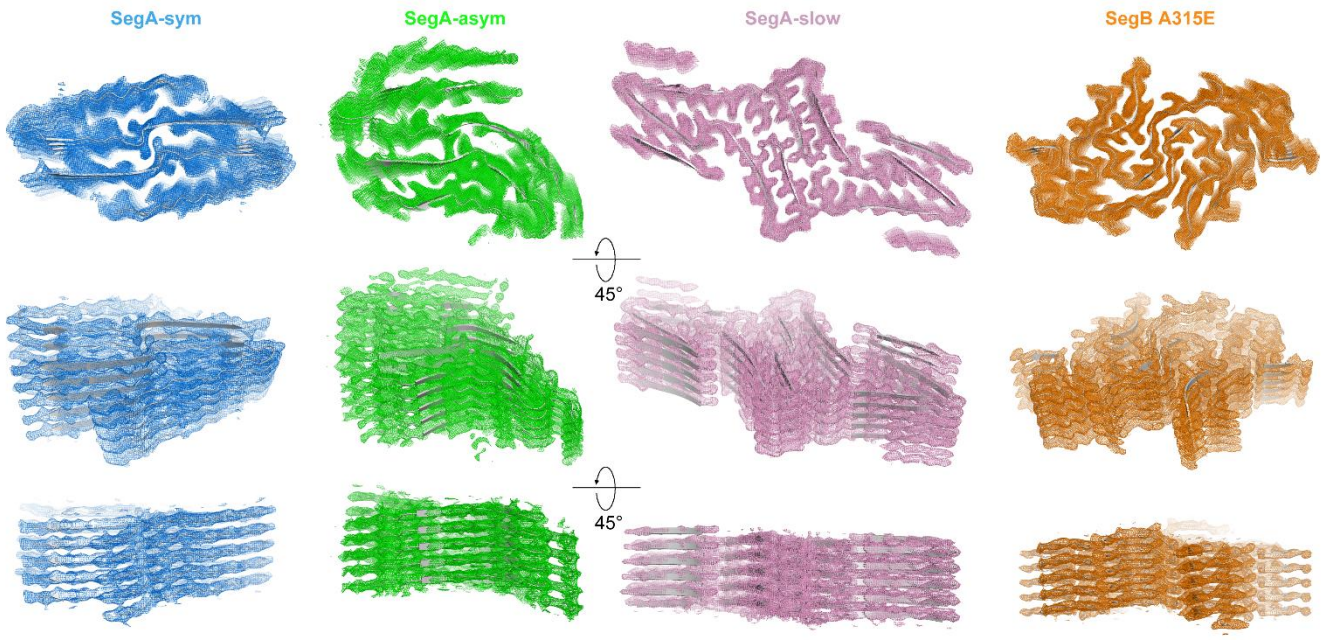

Supplementary Figure 4

Density maps of TDP-43 fibril structures.

Different views of the four structures reported in this study, with 5 layers of each structure shown. Density maps are shown in colored mesh and atomic model are shown in grey cartoons. Top-views demonstrate clear separation of beta-strands while tilted views demonstrate clear separation of the beta-sheets in the z-direction.

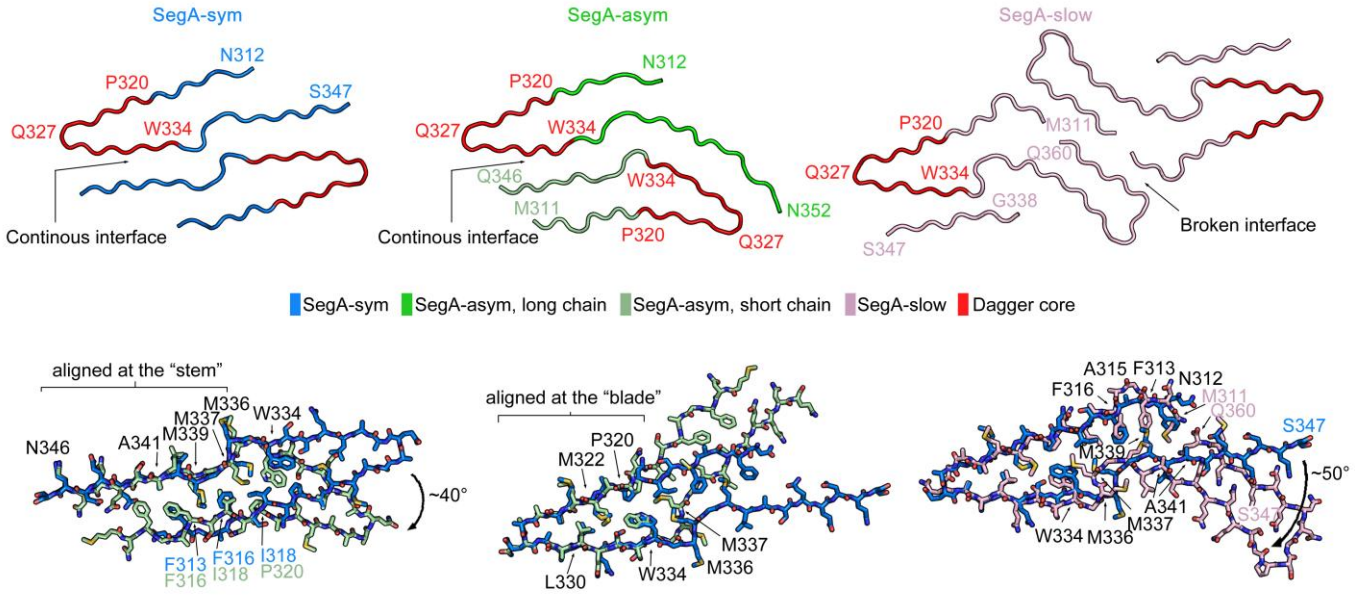

Supplementary Figure 5

Detailed analysis of the dagger-shaped fold.

(Upper panels) Three polymorphs of SegA are shown in cartoon and colored according to the color key. The core region of the dagger-shaped fold (residue 320-334) is colored red. (Bottom panels) Pairwise superposition of the dagger-shaped fold. (Left and middle) SegA-sym vs. SegA-asym short chain aligned at stem and dagger, respectively; (right) SegA-sym vs. SegA-slow. (Detailed alignment parameters are listed in Supplementary Table 2).

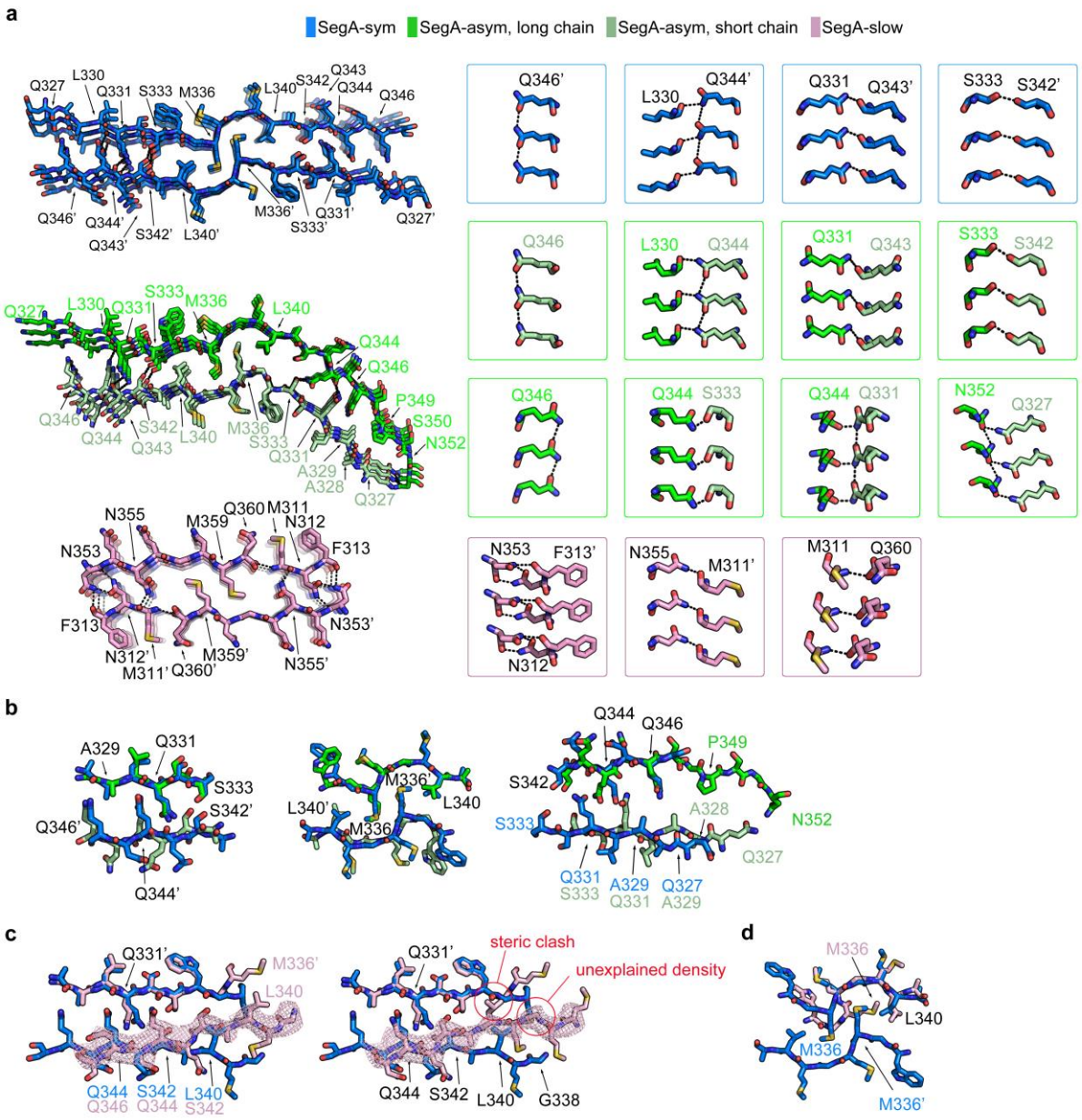

Supplementary Figure 6

Detailed analysis of the dimer interface in the dagger-shaped fold.

a, (Left column, from top to bottom) Cross-section of three layers of the continuous dimer interface in SegA-sym and SegA-asym, and broken interface in SegA-slow are shown. Side view of the detailed interactions of each interface are shown in the right columns. **b,** Superposition of continuous interface in SegA-sym and SegA-asym. Because of the 40° bend, we divided the continuous interface to three regions and performed superpositions separately. **c,** Model of the SegA-slow continuous interface with 2-residue different (left) or same (right) registration as in SegA-sym. Notice that the clash at Leu340 and unexplained density at Gly338 makes same registration model unfavorable. **d,** Conformational change of Met336 in SegA-slow block the Met336-Leu340 pocket of continuous interface shown in SegA-sym. Color coding in this figure is the same as in Figure 2, hydrogen bonds with distance between 2.3-3.2 Å are shown as black dashed lines. (Detailed alignment parameters are listed in Supplementary Table 2).

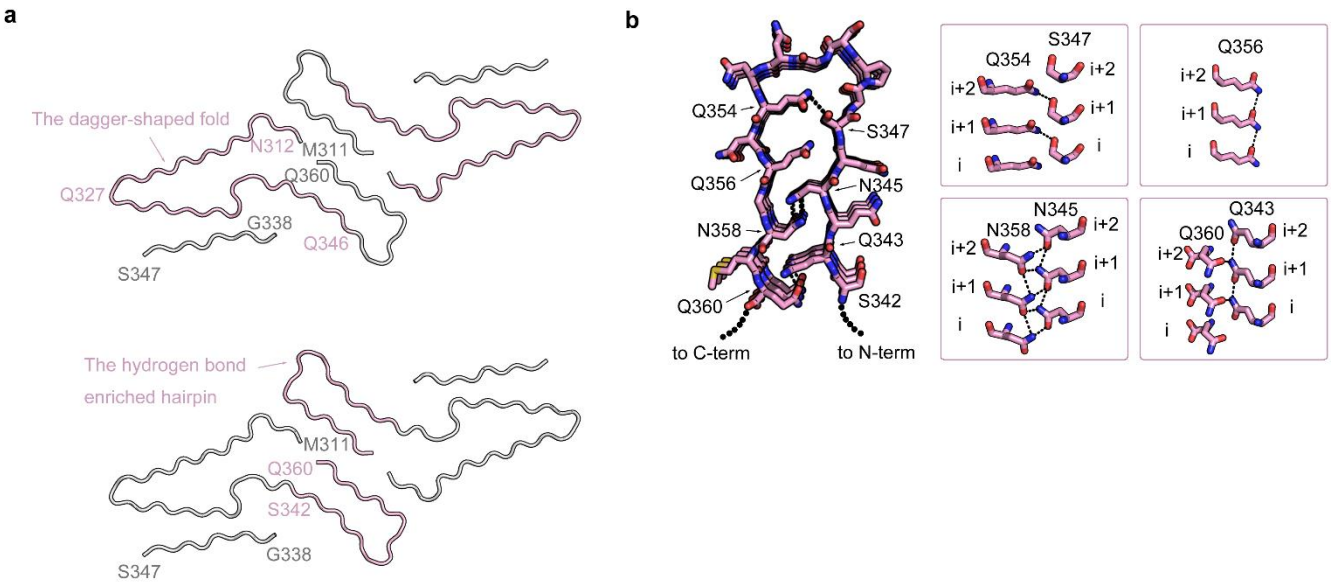

Supplementary Figure 7

The dagger-shaped fold and the hydrogen bond enriched hairpin structure in SegA-slow.

a, SegA-slow is shown in cartoon. The dagger-shaped fold (residue 312-346, upper panel) and the hydrogen bond enriched hairpin (residue 342-360, bottom panel) is colored pink, and the rest of the residues are colored gray. Note that both the dagger-shaped fold and the hydrogen bond enriched hairpin are individually compatible with full-length TDP-43 with free N- and C-terminals. **b,** Top view of hydrogen bond enriched hairpin structure in SegA-slow (left) and (right) side views of residues involved in hydrogen bond network.

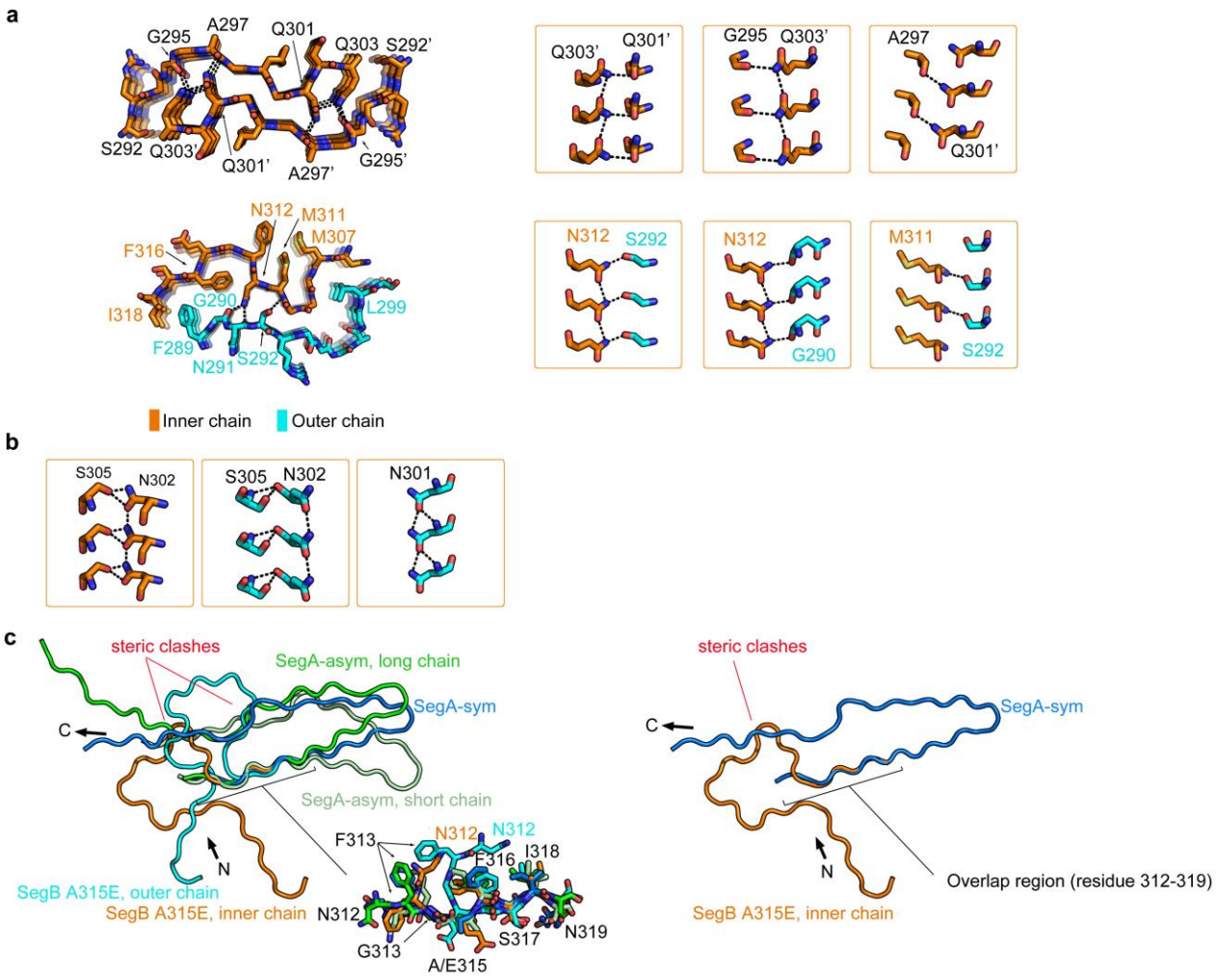

Supplementary Figure 8

Detailed analysis of the R-shaped fold.

a, (Left column, from top to bottom) Cross-section of three layers of the homodimer and heterodimer interfaces in SegB A315E are shown. Side view of the detailed interactions of each interface are shown in the right columns. **b,** Side view of hydrophilic interactions in the head of the R-shaped fold in the SegB A315E. **c,** Superposition of SegA and SegB A315E main chain models shows TDP-43 cannot simultaneously form a dagger-shaped fibril and an R-shaped fibril because of steric clashes; it must form either one or other. The simplified comparison using only SegA-sym to represent the dagger-shaped fold and SegB A315E inner chain to represent the R-shaped fold is shown in the right panel. Color coding in this figure is the same as in Figure 2; hydrogen bonds with distance between 2.3-3.2 Å are shown as black dashed lines. (Detailed alignment parameters are listed in Supplementary Table 2).

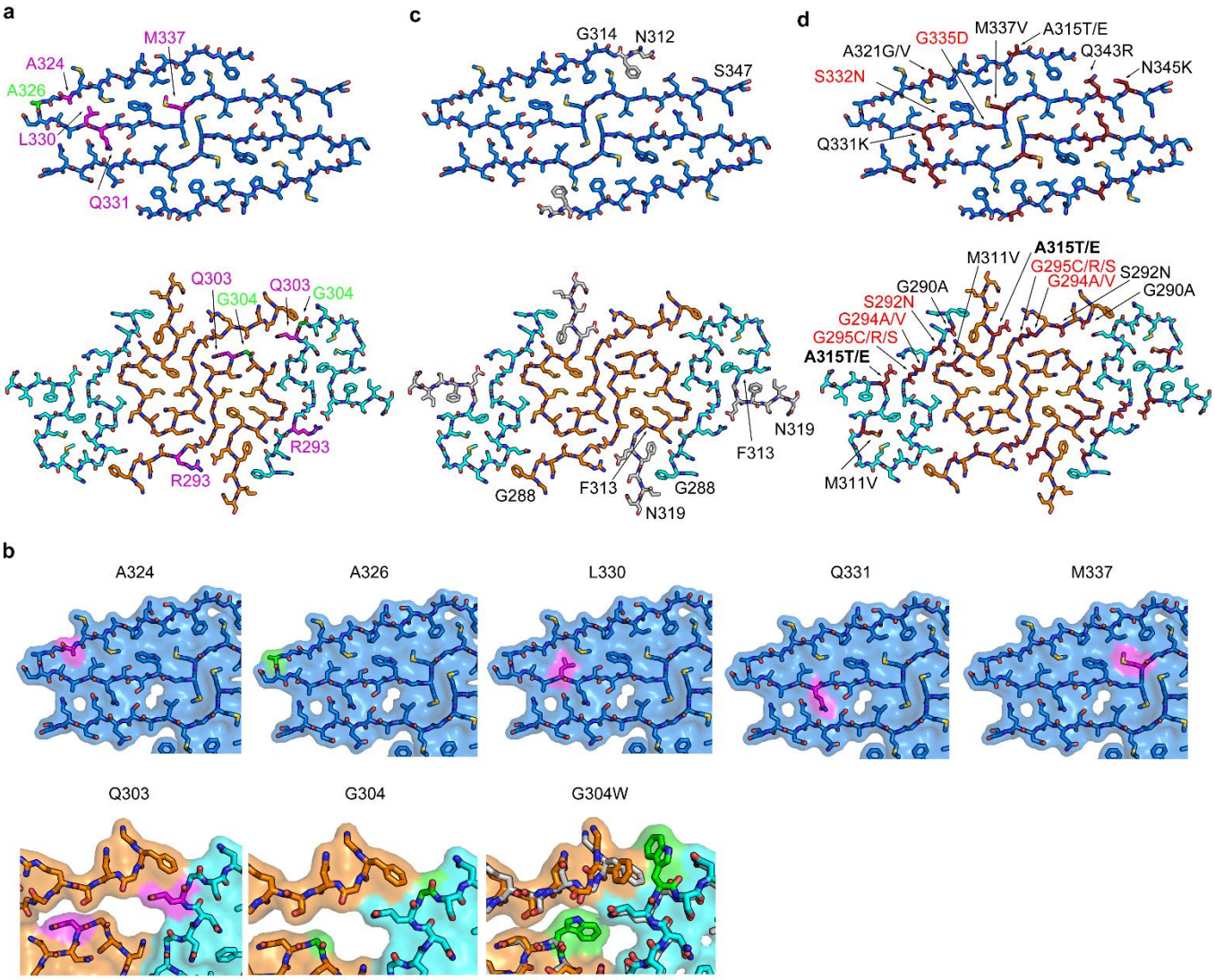

Supplementary Figure 9

Mutation analysis of TDP-43 fibril structures.

a & b, Residues tested in mutagenesis study in (top) SegA-sym and (bottom) SegB A315E. Residues that reduce pathological fragment TDP-CTF aggregation when mutated are shown in magenta and those that do not influence TDP-CTF aggregation when mutated are shown in green. Arg293 was mutated to glutamate and others were mutated to tryptophan. In (b), the models of both structures are shown in sticks and semitransparent surface mode. Notice that Ala324, Leu330, Gln331 and Met337 in SegA-sym and Gln303 in SegB A315E (also see Supplementary Figure 10) are in a tightly packed environment that does not tolerant a tryptophan mutation, consistent with our previous mutagenesis study where these mutations delayed the aggregation of the pathogenic TDP-43 fragment. In contrast, the Ala326 in SegA-sym and Gly304 in SegB A315E are in a relatively loose environment that is able to accommodate the tryptophan mutations, consistent with the result that A326W and G304W did not delay aggregation of the pathogenic TDP-43 fragment. For the G304W mutation, a plausible model of the R-shaped fold with G304W is shown in a separated panel. G304 from the inner chain and outer chain of SegB A315E were computationally mutated to tryptophan residues and phenix.real_space_refine was used to generate a model with acceptable rotamers and Ramachandran angles (Supplementary Table 3 and Supplementary Data Set 1). The mutated model is shown in color and the non-mutated model is shown in gray. This model helps explain the tolerance of the G304W mutation in our previous study. **c,** Synthetic TDP-43 peptide 274-313 and 314-353 were reported to seed TDP-43 aggregation in cells, and the overlapping region of these two peptides in SegA-sym (left, 314-347) and SegB A315E (right, 288-313) structures are shown in color, whereas missing residues from the synthetic peptides are shown in grey. Notice that these two peptides preserve most of the dagger-

and R-shaped folds making it likely that they adopt the same structures we report here. **d,** Positions of known hereditary mutations. The mutations compatible with the dagger- or R-shaped folds are colored black; the mutations potentially disruptive are colored red; the mutations favorable are bolded black.

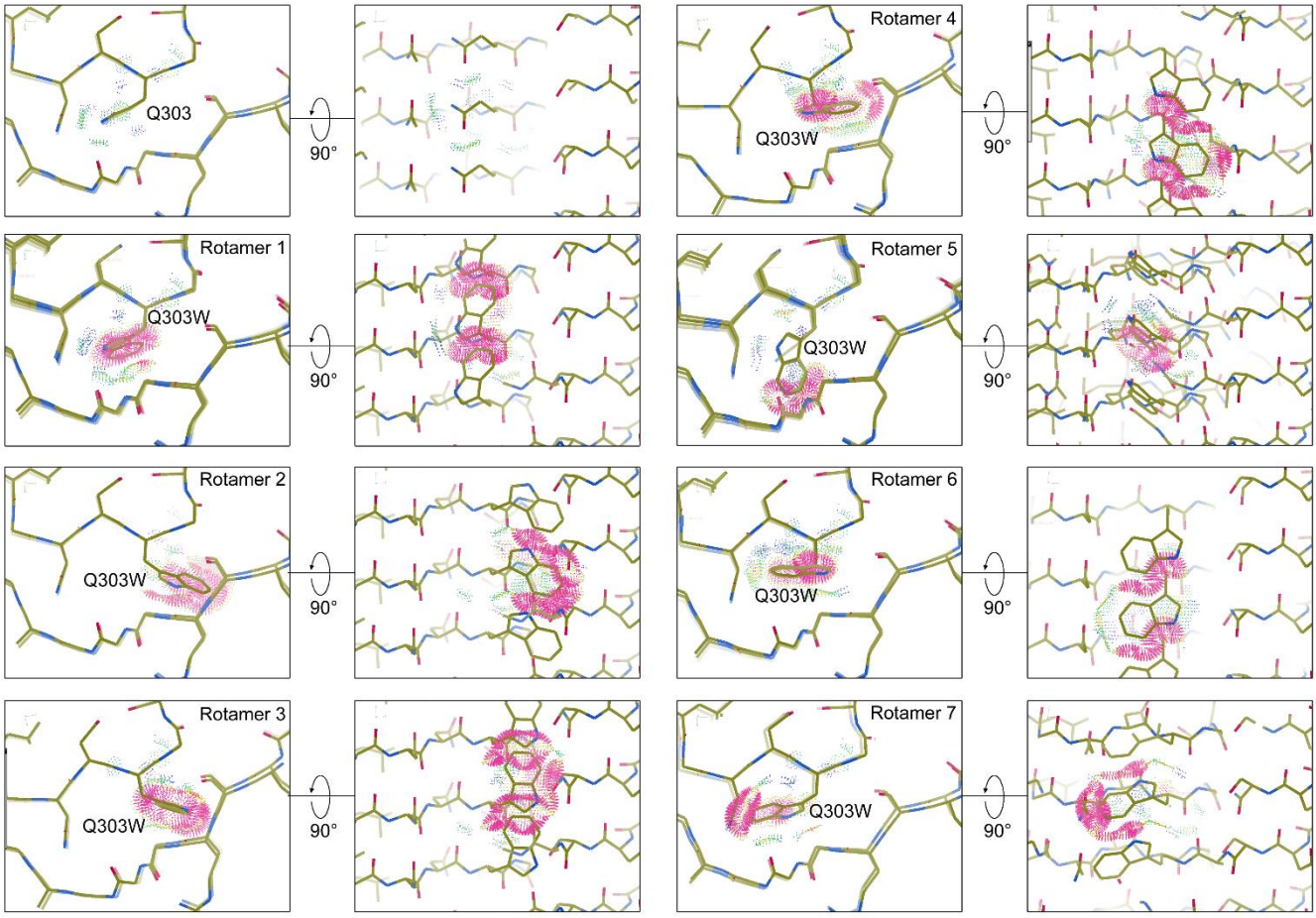

Supplementary Figure 10

Space limitation of Q303W in the R-shaped fold.

Gln303 in three continuous layers of the inner chain of the R-shaped fold was computationally mutated to tryptophan with all possible rotamers adopted. Steric clash was probed with COOT and displayed as red dots. Notice that the un-mutated Gln303 show no steric clash whereas all rotamers of Try303 show steric clash, indicating that Q303W is not compatible with the R-shaped fold.

Supplementary Table 1 Constructs designed in this study

Construct name	Residue range	Sequence
SUMO-TDP-43	1-414 (full length)	MGSSHHHHHHGSGLVPRGSASMSDSEVNQEAKPEVKPEVKPETHINL KVSDGSSEIFFKIKKTTPLRRLMEAFAKRQGKEMDSLRFLYDGIRIQAD QTPEDLDMEDNDIIEAHREQIGGMSEYIRVTEDENDEPIEIPSEDDGTV LLSTVTAQFPGACGLRYRNPVSQCMRGVRLVEGILHAPDAGWGNLV YVVNYPKDNKRKMDETDASSAVKVKRAVQKTSDLIVLGLPWKTTEQ DLKEYFSTFGEVLMVQVKKDLKTGHSKGFGFVRFTEYETQVKVMSQ RHMIDGRWCDCKLPNSKQSQDEPLRSRKVFVGRCTEDMTEDELREFF SQYGDVMDVFIPKPFRAFAFVTFADDQIAQSLCGEDLIIKGISVHISNA EPKHNSNRQLERSGRFGGNPGGFGNQGGFGNSRGGGAGLGNNQGSN MGGGMNFGAFSINPAMMAAAQAALQSSWGMMGMLASQQNQSGPS GNNQNQGNMQREPNQAFGSGNNSYSGSNSGAAIGWGSASNAGSGSG FNGGFGSSMDSKSSGWGM
SUMO-SegA	311-360	MGSSHHHHHHGSGLVPRGSASMSDSEVNQEAKPEVKPEVKPETHINL KVSDGSSEIFFKIKKTTPLRRLMEAFAKRQGKEMDSLRFLYDGIRIQAD QTPEDLDMEDNDIIEAHREQIGGMNFGAFSINPAMMAAAQAALQSSW GMMGMLASQQNQSGPSGNNQNQGNMQ
SUMO-SegB	286-331	MGSSHHHHHHGSGLVPRGSASMSDSEVNQEAKPEVKPEVKPETHINL KVSDGSSEIFFKIKKTTPLRRLMEAFAKRQGKEMDSLRFLYDGIRIQAD QTPEDLDMEDNDIIEAHREQIGGQGGFGNSRGGGAGLGNNQGSNMG GGMNFGAFSINPAMMAAAQAALQ
SUMO-SegB A315E	286-331	MGSSHHHHHHGSGLVPRGSASMSDSEVNQEAKPEVKPEVKPETHINL KVSDGSSEIFFKIKKTTPLRRLMEAFAKRQGKEMDSLRFLYDGIRIQAD QTPEDLDMEDNDIIEAHREQIGGQGGFGNSRGGGAGLGNNQGSNMG GGMNFGEFSINPAMMAAAQAALQ
SUMO-SegAB	286-360	MGSSHHHHHHGSGLVPRGSASMSDSEVNQEAKPEVKPEVKPETHINL KVSDGSSEIFFKIKKTTPLRRLMEAFAKRQGKEMDSLRFLYDGIRIQAD QTPEDLDMEDNDIIEAHREQIGGQGGFGNSRGGGAGLGNNQGSNMG GGMNFGAFSINPAMMAAAQAALQSSWGMMGMLASQQNQSGPSGN NQNQGNMQ

Supplementary Table 2 Structural alignment details

Figure #	Residues displayed	Residues aligned	# atom pairs	r.m.s.d.
Figure 2a&c	SegA-sym 312-347 & SegA-asym long chain 312-352	312-336	161	1.344
Figure 2f	SegB A315E inner chain & outer chain	288-319	177	2.243
Figure 2a & Supplementary Figure 5a bottom left	SegA-sym 312-347 & SegA-asym short chain 311-346	336-346	70	1.150
Figure 2a & Supplementary Figure 5a bottom middle	SegA-sym 312-347 & SegA-asym short chain 311-346	322-336	88	1.222
Figure 2a & Supplementary Figure 5a bottom right	SegA-sym 312-347 & SegA-slow 311-360	312-336	150	1.776
Supplementary Figure 5c left	SegA-sym 328-333, 341'-346' & SegA-asym long chain 328-333, short chain 341-346	328-333	35	0.810
Supplementary Figure 5c middle	SegA-sym 334-341 both chains & SegA-asym 334-341 both chains	(long chain) 334-341	45	0.873
Supplementary Figure 5c right	SegA-sym 342-347, 327'-333' & SegA-asym long chain 342-352, short chain 327-333	342-347	44	1.568
Supplementary Figure 5d	SegA-sym 328-336, 338'-347' & SegA-slow long chain 328-336, short chain 338-347	328-336	53	0.624
Supplementary Figure 5e	SegA-sym 334-341 both chains & SegA-slow long chain 334-341	336-340	27	0.948
Supplementary Figure 5h (enlarged)	SegA-sym (312-319) & SegB A315E inner chain (312-319)	312-319	39	1.056
Supplementary Figure 5h (enlarged)	SegA-asym long chain (312-319) & SegB A315E inner chain (312-319)	312-319	43	1.463
Supplementary Figure 5h (enlarged)	SegA-asym short chain (312-319) & SegB A315E inner chain (312-319)	312-319	44	1.343
Supplementary Figure 5h (enlarged)	SegB outer chain (312-319) & SegB A315E inner chain (312-319)	315-319	35	1.573

Supplementary Table 3 Validation statistics of the hypothetical SegB A315E G304W model

	SegB A315E G304W (hypothetical model)
R.m.s.d. bonds (Å)	0.007
R.m.s.d. angles (°)	0.574
Molprobity clashscore, all atoms	16.61
Molprobity score	2.47
Poor rotamers (%)	0
Ramachandran outliers (%)	0
Ramachandran allowed (%)	21.8
Ramachandran favoured (%)	79.2
Cβ deviations > 0.25 Å (%)	0
Bad bonds (%)	0
Bad angles (%)	0